

Study of the interaction between sodium salts of (2*E*)-3-(4'-halophenyl)prop-2-enoyl sulfachloropyrazine and bovine serum albumin by fluorescence spectroscopy

Xuan Luo, Chuanrong Du, Jinrui Wei, Jiang Deng, Yijie Lin and Cuiwu Lin*

ABSTRACT: Three sodium salts of (2*E*)-3-(4'-halophenyl)prop-2-enoyl sulfachloropyrazine (CCSCP) were synthesized and their structures were determined by ¹H and ¹³C NMR, LC-MS and IR. The binding properties between CCSCPs and bovine serum albumin (BSA) were studied using fluorescence spectroscopy in combination with UV-vis absorbance spectroscopy. The results indicate that the fluorescence quenching mechanisms between BSA and CCSCPs were static quenching at low concentrations of CCSCPs or combined quenching (static and dynamic) at higher CCSCP concentrations of 298, 303 and 308 K. The binding constants, binding sites and corresponding thermodynamic parameters (ΔH , ΔS , ΔG) were calculated at different temperatures. All ΔG values were negative, which revealed that the binding processes were spontaneous. Although all CCSCPs had negative ΔH and positive ΔS , the contributions of ΔH and ΔS to ΔG values were different. When the 4'-substituent was fluorine or chlorine, van der Waals interactions and hydrogen bonds were the main interaction forces. However, when the halogen was bromine, ionic interaction and proton transfer controlled the overall energetics. The binding distances between CCSCPs and BSA were determined using the Förster non-radiation energy transfer theory and the effects of CCSCPs on the conformation of BSA were analyzed by synchronous fluorescence spectroscopy. Copyright © 2012 John Wiley & Sons, Ltd.

Keywords: halo-cinnamic acid; sulfachloropyrazine; bovine serum albumin; fluorescence spectroscopy; interaction

Introduction

Since 2006, our laboratory has been interested in an herbal medicine with procoagulant and haemostatic activities, namely *Blumea riparia* (BL) DC. (Compositae). It has been used in China to treat gynaecological diseases including menorrhagia, puerperal metrorrhagia, peripheral oedema, infertility and vulvar ulcer (1). According to our previous research, its major procoagulant and haemostatic components are phenolic acids, including vanillic acid, syringic acid, *p*-coumaric acid, caffeic acid and protocatechuic acid (2). These phenolic acid compounds had (2*E*)-3-phenylprop-2-enoyl or benzoyl frameworks. Our goal was to make structure modifications of (2*E*)-3-phenylprop-2-enoic or benzoic acids to find other compounds with better procoagulant and haemostatic activities. At the same time, we introduced sulphonamides (SAs) onto (2*E*)-3-phenylprop-2-enoyl or benzoyl frameworks to give these compounds anti-inflammatory or antimicrobial activities.

Drug properties such as absorption, distribution, metabolism, excretion, stability and toxicity during the chemotherapeutic process are very important. These properties are strongly affected by drug-protein complexes. Therefore, the interaction between drug and protein and the study of their biological mechanism have recently become a focus of research (3–5). Choosing a good protein model is crucial. Serum albumin, the major soluble protein constituent in the circulatory system of a wide variety of organisms, has many important biological functions. One of them is to reversibly bind to a large variety of endogenous and exogenous ligands such as fatty acids, drugs

and metal ions in the bloodstream (6,7). Because bovine serum albumin (BSA) and human serum albumin (HSA) display approximately 76% sequence homology and the 3D structure of BSA is believed to be similar to that of HSA (8,9), BSA was selected as our protein model.

In the present work, three sodium salts chosen from: (2*E*)-3-(4'-halophenyl)prop-2-enoyl sulfachloropyrazine (CCSCP); (2*E*)-N-{4'-[(6'''-chloropyrazin-2'''-yl)sulfamoyl]phenyl}-3-(4'-fluorophenyl)prop-2-enamide sodium salt (PFCCSCP); (2*E*)-3-(4'-chlorophenyl)-N-{4'-[(6'''-chloropyrazin-2'''-yl)sulfamoyl]phenyl}prop-2-enamide sodium salt (PCCSCP); and (2*E*)-3-(4'-bromophenyl)-N-{4'-[(6'''-chloropyrazin-2'''-yl)sulfamoyl]phenyl}prop-2-enamide sodium salt (PBCCSCP) (Figure 1) were synthesized and the interaction with BSA was studied using fluorescence and absorption spectroscopy. The binding constants, basic thermodynamic parameters and binding distances were obtained. At the same time, the effects of different halogens of the benzene ring on the binding properties of CCSCPs to BSA were explored. We believe that the study provides valuable information for drug design and pharmaceutical research.

* Correspondence to: Cuiwu Lin, 100 Daxue Dong Road, School of Chemistry and Chemical Engineering, Guangxi University, Nanning, Guangxi, 530005, P. R. China. E-mail: cuiwulin@163.com

School of Chemistry and Chemical Engineering, Guangxi University, Nanning, Guangxi, 530004, People's Republic of China

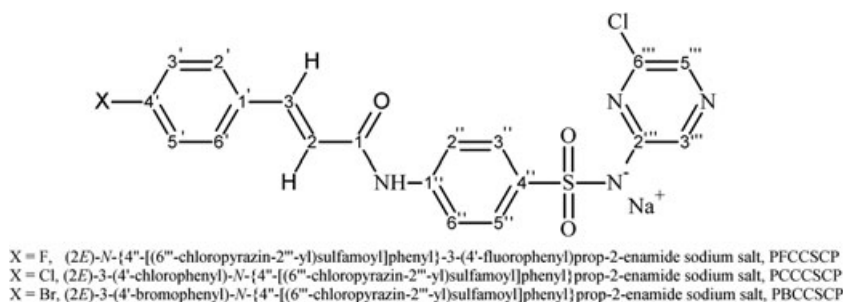


Figure 1. Structures of sodium salts of (2E)-3-(4'-halophenyl)prop-2-enoyl sulfachloropyrazine

Experimental

Apparatus

Melting points were measured on an X-4 microscopic melting point apparatus made by Beijing Tech Instruments. All pH measurements were made with a pHs-3C digital pH meter (Shanghai Leici Device Works, China) with a combined glass-calomel electrode. The absorption and IR spectra were obtained using a Unico (China) UV-2102PCS and Bruker Tensor27, respectively. Fluorescence spectra were recorded on a Shimadzu RF-5301 fluorescence spectrophotometer (Tokyo, Japan) with a 1-cm quartz cell and thermostatic cuvette holder. The excitation and emission bandwidths were both 5 nm. The temperature of the samples was maintained by recycling water throughout the experiment. ^1H and ^{13}C NMR spectra were recorded on a Bruker Advance III 300 at 300 MHz for ^1H and 75 MHz for ^{13}C , respectively in $\text{DMSO}-d_6$. Chemical shifts are given in δ (ppm) and coupling constants in Hz. ESI-MS was obtained on a Shimadzu LC-MS 2010A.

Reagents

A pH 7.4 buffer solution was prepared as follows: 6.0 g tris (hydroxymethyl)aminomethane and 4.5 g NaCl (Sinopharm Group Chemical Reagent Co., Ltd, China) were dissolved in 1 L distilled water and then 3 M hydrochloric acid solution was used to adjust the pH to 7.4. BSA (Sigma-Aldrich) was dissolved daily in 0.1 M Tris-HCl buffer (pH=7.4) to prepare a stock solution (1.0×10^{-4} M) and stored in a refrigerator. CCSCP stock solutions (1×10^{-3} M) were prepared by dissolving 0.025 mmol derivatives in 15 mL DMSO and diluting in a 25 mL volumetric flask by tris-HCl buffer. Working solutions were prepared daily as follows: 0–180 μL CCSCP stock solutions and 1 mL BSA solution were added into a 10 mL comparison tube and diluted with buffer. All other chemicals were purchased from Nanning Lantian Experiment Equipment Co., Ltd (Nanning, Guangxi, China) and were used without purification.

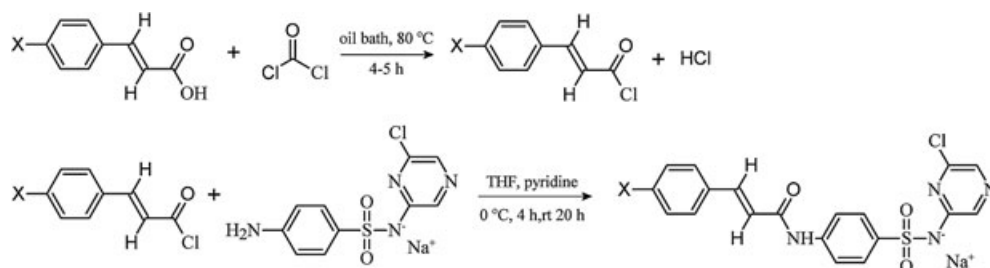
Procedures

General procedure for the syntheses of CCSCPs. CCSCPs were synthesized from *p*-halogenated cinnamic acids and sodium [(4-aminophenyl)sulfonyl](6-chloropyrazin-2-yl)azanide. The synthesis route is shown in Scheme 1. After the reaction, the mixture was transferred to 1 L beakers and made up to 1 L with distilled water to precipitate the products. The raw products were separated by vacuum filtration and recrystallized in methanol-THF or methanol-EtOAc solvent systems.

CCSCP-BSA interaction study. Fluorescence measurements were carried out by successive addition of 1×10^{-3} M CCSCP stock solutions to a fixed amount of BSA to give a final concentration of 1×10^{-5} M in each 10 mL comparison tube. The final volume was 10.0 mL with the buffer. Thus, a series of solutions containing different amount of CCSCPs and a definite amount of BSA were obtained. The solutions were held in a thermostat water bath for 10 min before fluorescence measurements. Fluorescence emission spectra were read in a range of wavelengths from 300–450 nm using an excitation wavelength of 295 nm. All experiments were performed at three temperatures (298, 303 and 308 K). Synchronous fluorescence spectra of BSA (1×10^{-5} M) in the presence of CCSCPs (0.2 – 1.8×10^{-5} M) were recorded. The wavelength ranges of synchronous scanning were from 280–350 nm ($\Delta\lambda = 15$ nm) and 290–400 nm ($\Delta\lambda = 60$ nm) at 298 K.

Sodium salt of (2E)-N-{4'-[(6'''-Chloropyrazin-2'''-yl)sulfamoyl]phenyl}-3-(4'-fluorophenyl)prop-2-enamide (PFCCSCP)

Light yellow needle crystals from the above recrystallization had a melting point of 278–279°C, an ESI-MS of m/z 431.1 (calcd 431.8 for $\text{C}_{19}\text{H}_{13}\text{ClFN}_4\text{O}_3\text{S}$); IR (KBr) ν_{max} 3267 (vw, $-\text{NH}-\text{SO}_2-$), 3115 (w, $-\text{NH}-\text{CO}-$), 1690 (s, $>\text{C}=\text{O}$), 1633 (s, $>\text{C}=\text{C}-\text{H}$), 1600–1300 (m to s, Ar-H), 1343 and 1191 (vs, $>\text{S}=\text{O}$), 1232 (m, F-Ph) and 1092 (m, Cl-Ar) cm^{-1} for ^1H and ^{13}C NMR spectroscopic data ($\text{DMSO}-d_6$) (Tables 1 and 2).



Scheme 1. Synthesis route of sodium salts of (2E)-3-(4'-halophenyl)prop-2-enoyl sulfachloropyrazine

Table 1. Assignments of CCSCPs ¹H NMR data

Position	PFCCSCP (δ_{H} , mult., J, Hz)	PCCCSKP (δ_{H} , mult., J, Hz)	PBCCSCP (δ_{H} , mult., J, Hz)
2	6.767 (d, 16.2)	6.821 (d, 15.7)	6.833 (d, 15.8)
3	7.632 (d, 16.2)	7.668 (d, 15.7)	7.597 (d, 15.8)
2'	7.706 (m, 8.9, 5.5, 2.0)	7.655 (ddd, 8.6, 2.4, 1.9)	7.632 (ddd, 8.7, 2.0, 1.9)
3'	7.288 (m, 8.9, 2.0)	7.490 (ddd, 8.6, 2.4, 1.9)	7.578 (ddd, 8.7, 2.0, 1.9)
5'	7.288 (m, 8.9, 2.0)	7.490 (ddd, 8.6, 2.4, 1.9)	7.578 (ddd, 8.7, 2.0, 1.9)
6'	7.706 (m, 8.9, 5.5, 2.0)	7.655 (ddd, 8.6, 2.4, 1.9)	7.632 (ddd, 8.7, 2.0, 1.9)
2''	7.953 (ddd, 9.3, 2.2, 1.8)	7.961 (ddd, 9.1, 2.1, 1.9)	7.957 (ddd, 9.1, 2.2, 2.0)
3''	7.887 (ddd, 9.3, 2.2, 1.8)	7.892 (ddd, 9.1, 2.1, 1.9)	7.888 (ddd, 9.1, 2.2, 2.0)
5''	7.887 (ddd, 9.3, 2.2, 1.8)	7.892 (ddd, 9.1, 2.1, 1.9)	7.888 (ddd, 9.1, 2.2, 2.0)
6''	7.953 (ddd, 9.3, 2.2, 1.8)	7.961 (ddd, 9.1, 2.1, 1.9)	7.957 (ddd, 9.1, 2.2, 2.0)
3'''	8.332 (d, 0.6)	8.321 (d, 0.37)	8.315 (d, 0.37)
5'''	8.292 (d, 0.6)	8.294 (d, 0.37)	8.289 (d, 0.37)
-CO-NH-	10.632 (s)	10.668 (s)	10.671 (s)

Table 2. Assignments of CCSCPs ¹³C NMR data

Position	PFCCSCP	PCCCSKP	PBCCSCP
1	164.1	164.0	164.0
2	121.5, 121.5 (⁶ J _{C-F} = 2.1)	122.4	122.5
3	143.8	143.7	143.7
1'	131.2, 131.1 (⁴ J _{C-F} = 3.2)	134.6	133.8
2'	130.2, 130.1 (³ J _{C-F} = 8.5)	129.6	132.1
3'	116.2, 116.0 (² J _{C-F} = 22.1)	129.2	129.9
4'	164.7, 161.5 (¹ J _{C-F} = 248.2)	133.5	123.4
5'	116.2, 116.0 (² J _{C-F} = 22.1)	129.2	129.9
6'	130.2, 130.1 (³ J _{C-F} = 8.5)	129.6	132.1
1''	132.9	133.0	133.1
2''	118.9	118.9	118.9
3''	129.0	129.0	129.0
4''	132.3	132.3	132.4
5''	129.0	129.0	129.0
6''	118.9	118.9	118.9
2'''	137.1	137.1	137.0
3'''	145.5	145.5	145.6
5'''	147.5	147.5	147.6
6'''	140.2	140.0	140.1

Sodium salt of (2E)-3-(4'-Chlorophenyl)-N-{4''-[(6'''-chloropyrazin-2'''-yl)sulfamoyl] phenyl}prop-2-enamide (PCCCSKP)

The white powder from the above recrystallization had a melting point of 282–283°C; ESI-MS *m/z* 448.1 (calcd 448.3 for C₁₉H₁₃Cl₂N₄O₃S); IR (KBr) ν_{max} 3266 (vw, -NH-SO₂-), 3116 (m, -NH-CO-), 1688 (m, > C=O), 1631 (m, > C=C-H), 1600–1300 (m to vs, Ar-H), 1339 and 1163 (vs, > S=O), 1091 (m, Cl-Ar) cm⁻¹ for ¹H and ¹³C NMR spectroscopic data (DMSO-*d*₆) Tables 1 and 2).

Sodium salt of (2E)-3-(4'-Bromophenyl)-N-{4''-[(6'''-chloropyrazin-2'''-yl)sulfamoyl] phenyl}prop-2-enamide (PBCCSCP)

The white powder from the above recrystallization had a melting point of 282–283°C; ESI-MS *m/z* 493.1 (calcd 492.8 for C₁₉H₁₃BrClN₄O₃S); IR (KBr) ν_{max} 3267 (vw, -NH-SO₂-), 3115 (m, -NH-CO-), 1689 (m, > C=O), 1632 (m, > C=C-H), 1600–1300 (m to vs, Ar-H), 1339 and 1163 (vs, > S=O), 1093 (m, Cl-Ar) cm⁻¹ for ¹H and ¹³C NMR spectroscopic data (DMSO-*d*₆) (Tables 1 and 2).

Results and discussion

Fluorescence quenching study

Fluorescence quenching refers to any process that decreases the fluorescence intensity of a fluorophore by a variety of molecular interactions with a quencher molecule, including excited-state reactions, molecular rearrangements, energy transfer, ground-state complex formation and collisional quenching processes. Due to different mechanisms, quenching can be classified as either dynamic or static. Dynamic or collisional quenching results from collision between a fluorophore and a quencher; static quenching is due to the formation of ground-state complex between a fluorophore and a quencher. In general, dynamic and static quenching can be distinguished by their different dependence on temperature and viscosity. The quenching rate constants decrease with increasing temperature for static quenching but the reverse effect is observed for dynamic quenching (10).

The fluorescence spectra of BSA in the presence of different amounts of PFCCSCP, PCCCSKP and PBCCSCP at 298 K are shown in Figure 2. As can be seen, the fluorescence intensity of BSA consistently decreased upon increasing the concentrations of CCSCPs, which indicated that CCSCPs could interact with BSA. Furthermore, the maximum wavelength of BSA shifted from 344 to 357 nm regardless of PFCCSCP, PCCCSKP or PBCCSCP after the addition of each of the CCSCPs. A slight red shift of fluorescence spectrum indicated that the tyrosine residue was brought to a more hydrophilic environment (10) with strengthened hydrogen bonding (11) in the BSA-CCSCP systems. The structure of the hydrophobic subdomain where tryptophan was placed was not compact and the segment of polypeptide changed its conformation to a more extended state after the addition of CCSCPs (12,13).

To confirm the quenching mechanism, fluorescence quenching data were analyzed by the Stern-Volmer equation (equation 1):

$$\frac{F_0}{F} = 1 + K_{SV}[Q] = 1 + k_q\tau_0[Q] \quad (1)$$

where *F*₀ and *F* are the fluorescence intensity of BSA in the absence or presence of quencher, respectively; *K*_{SV} is the Stern-Volmer quenching constant; [Q] is the quencher concentration; *k*_q is the bimolecular quenching constant; τ_0 is the average lifetime of the molecule without quencher and its value is considered to be 10⁻⁸ s (4,10).

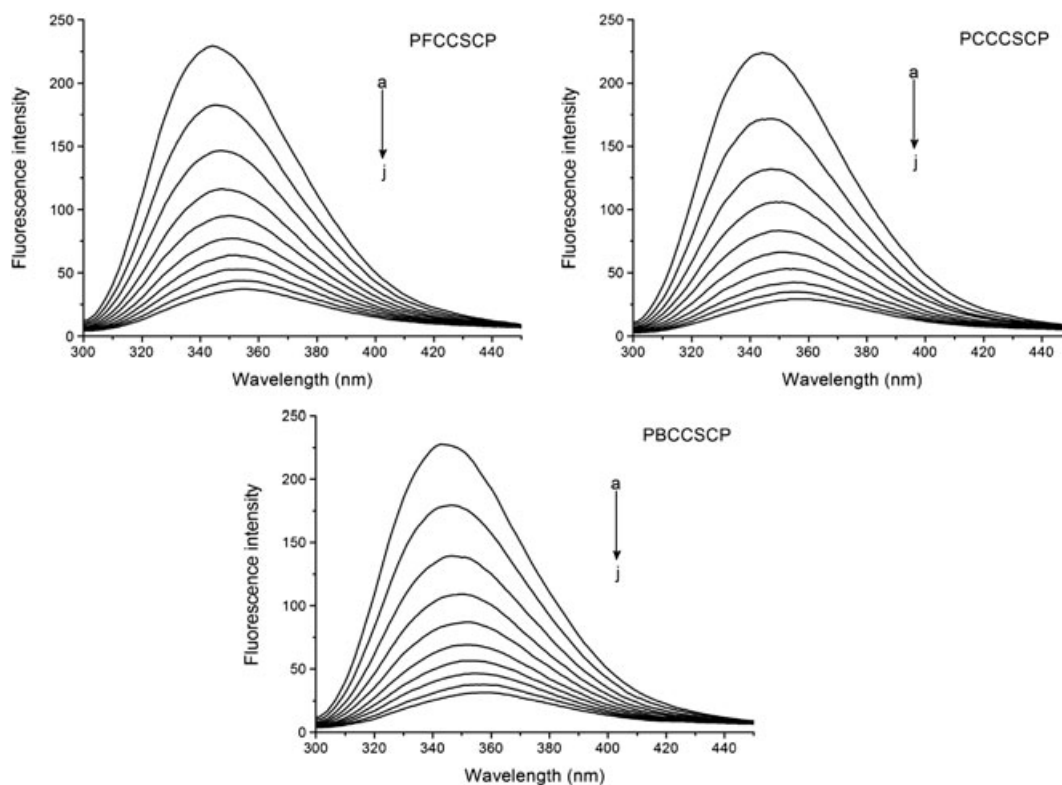


Figure 2. Fluorescence quenching spectra of BSA at different concentrations of CCSCPs at 298 K, $\lambda_{\text{ex}} = 295$ nm; $c(\text{BSA}) = 1.00 \times 10^{-5}$ M; $c(\text{CCSCP}) / (\times 10^{-5} \text{ M})$, (a–j) 0.00, 0.20, 0.40, 0.60, 0.80, 1.00, 1.20, 1.40, 1.60 and 1.80, respectively

In many instances, the fluorophore could be quenched both by collisions and by complex formation with the same quencher. The characteristic feature of the Stern-Volmer plots in such circumstances had an upward curvature. The modified Stern-Volmer equation (2) better accounted for the upward curvature observed when both static and dynamic quenching occurred for the same fluorophore;

$$\frac{F_0}{F} = (1 + K_D[Q])(1 + K_S[Q]) = 1 + (K_D + K_S)[Q] + K_D K_S [Q]^2 \quad (2)$$

where K_D and K_S are the dynamic and static quenching constants, respectively. The modified equation was second order with respect to $[Q]$, which led to the upward curvature observed at higher $[Q]$ (4,10).

The Stern-Volmer plots of the quenching of BSA fluorescence by CCSCPs at different temperatures are displayed in Figure 3. As can be seen, the plots F_0/F for $[Q]$ ranging from 0.20 to 1.80×10^{-5} M of CCSCPs concaved toward the y-axis either at low or high temperatures. The fluorescence quenching data were analyzed according to equation (2) at all three temperatures and had good linearity (for PFCCSCP, $R_{298}^2 \kappa = 0.9998$, $R_{303}^2 \kappa = 0.9992$, $R_{308}^2 \kappa = 0.9996$; for PCCCSQP, $R_{298}^2 \kappa = 0.9998$, $R_{303}^2 \kappa = 0.9996$, $R_{308}^2 \kappa = 0.9990$; for PBCCSCP, $R_{298}^2 \kappa = 0.9994$, $R_{303}^2 \kappa = 0.9986$, $R_{308}^2 \kappa = 0.9995$). Meanwhile, the plots (inserts in Figure 3) of F_0/F for BSA versus $[Q]$ at low concentrations of CCSCPs (0.20 to 1.00×10^{-5} M) at three temperatures based on equation (1) exhibited good linearity and the values of K_{SV} and k_q are illustrated in Table 3. The phenomena could indicate that a single quenching mechanism, either dynamic or static quenching, occurred at lower concentrations of CCSCPs at 298, 303 and 308 K. However, a combined quenching (static and dynamic) process occurred at higher concentrations of CCSCPs at all three temperatures.

k_q reflects the efficiency of quenching or the accessibility of the fluorophore to the quencher. The diffusion-controlled quenching typically resulted in values of k_q near $1.0 \times 10^{10} \text{ M}^{-1} \cdot \text{s}^{-1}$ (10). The results in Table 3 show that the values for k_q were much greater than the diffusion-controlled value. With the rising temperature, K_{SV} decreased for PFCCSCP and PCCCSQP and increased for PBCCSCP. Therefore, the fluorescence quenching of PFCCSCP and PCCCSQP could be a static quenching process at low concentrations rather than a dynamic quenching process. For PBCCSCP, K_{SV} increased with the rising temperature but the increment was very small (less than 1%). At the same time, its k_q was more than 2500x the maximum diffusion collision quenching rate constant ($1.0 \times 10^{10} \text{ M}^{-1} \cdot \text{s}^{-1}$). Therefore, PBCCSCP fluorescence quenching could be a static quenching process at low concentrations as well.

Binding constants and binding sites

When small molecules bind independently to a set of equivalent sites on a macromolecule, the binding constant (K_A) and the number of binding sites (n) can be determined by the following equation (3):

$$\lg\left(\frac{F_0 - F}{F}\right) = \lg K_A + n \lg [Q] \quad (3)$$

However, this equation can only calculate the binding constant and the number of binding sites for static quenching processes (14). Double reciprocal curves of fluorescence quenching of CCSCPs were plotted (Figure 4) in the same concentration range based on equation (3). The values of K_A and n listed in Table 4 were determined from the slope and the intercept. The

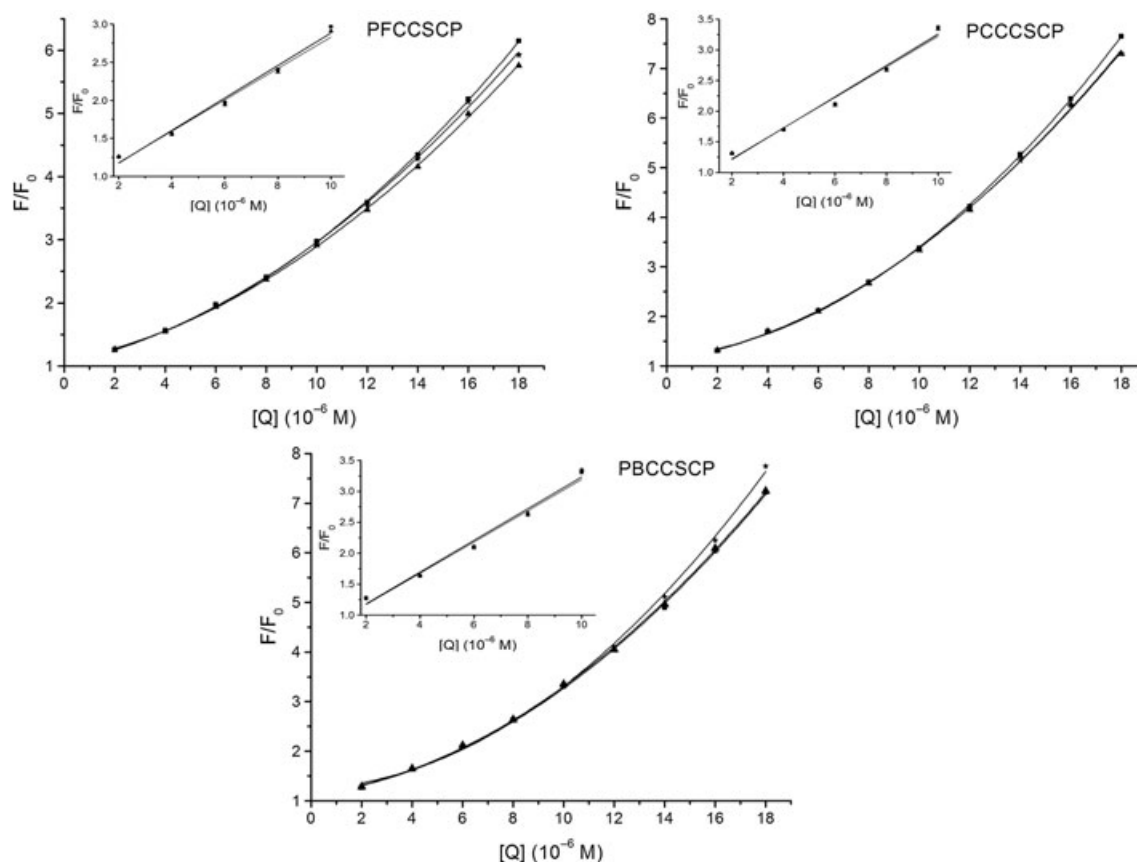


Figure 3. Stern–Volmer plots of the fluorescence quenching of BSA by CCSCPs at different temperatures (■, 298 K; ●, 303 K; ▲, 308 K)

Table 3. Quenching constants of BSA by CCSCP at different temperatures

		BSA–PFCCSCP	BSA–PCCCSCP	BSA–PBCCSCP
T = 298 K	$K_{SV} \times 10^5 \text{ (M}^{-1}\text{)}$	2.13(13)	2.57(18)	2.53(18)
	$k_q \times 10^{13} \text{ (M}^{-1}\cdot\text{s}^{-1}\text{)}$	2.13(13)	2.57(18)	2.53(18)
	R	0.9943	0.9923	0.9928
T = 303 K	$K_{SV} \times 10^5 \text{ (M}^{-1}\text{)}$	2.13(14)	2.54(17)	2.56(18)
	$k_q \times 10^{13} \text{ (M}^{-1}\cdot\text{s}^{-1}\text{)}$	2.13(14)	2.54(17)	2.56(18)
	R	0.9935	0.9935	0.9925
T = 308 K	$K_{SV} \times 10^5 \text{ (M}^{-1}\text{)}$	2.06(14)	2.50(18)	2.56(19)
	$k_q \times 10^{13} \text{ (M}^{-1}\cdot\text{s}^{-1}\text{)}$	2.06(14)	2.50(18)	2.56(19)
	R	0.9936	0.9919	0.9922

results showed that there was strong binding between CCSCPs and BSA, which means that CCSCPs could be stored and carried by protein in the body. The binding constants of the interaction followed the order: PBCCSCP > PCCCSCP > PFCCSCP at all three temperatures. This means that PBCCSCP had the strongest ability to bind BSA. Furthermore, the binding constants decreased with rising temperatures, which confirms that their fluorescence quenching was static.

Thermodynamic analysis and the interaction forces between BSA and CCSCPs

On the basis of the thermochemical behaviour of small molecule interactions, the interaction force between small molecules and macromolecules include hydrophobic, electrostatic and van der

Waals interactions, hydrogen bonds (15). The thermodynamic parameters were determined using van't Hoff equation (4):

$$\ln K_A = -\frac{\Delta H}{RT} + \frac{\Delta S}{R} \quad (4)$$

where K_A is the binding constant at the corresponding temperature T , R is the gas constant, T is absolute temperature, ΔH is enthalpy change and ΔS is entropy change. The $\ln K_A$ versus $1/T$ plot enabled the determination of ΔH and ΔS . The value of enthalpy free energy change (ΔG) was calculated from equation (5):

$$\Delta G = \Delta H - T\Delta S = -RT \ln K_A \quad (5)$$

The binding studies were carried out at 298, 303 and 308 K and the values are given in Table 5. All ΔG values no matter at

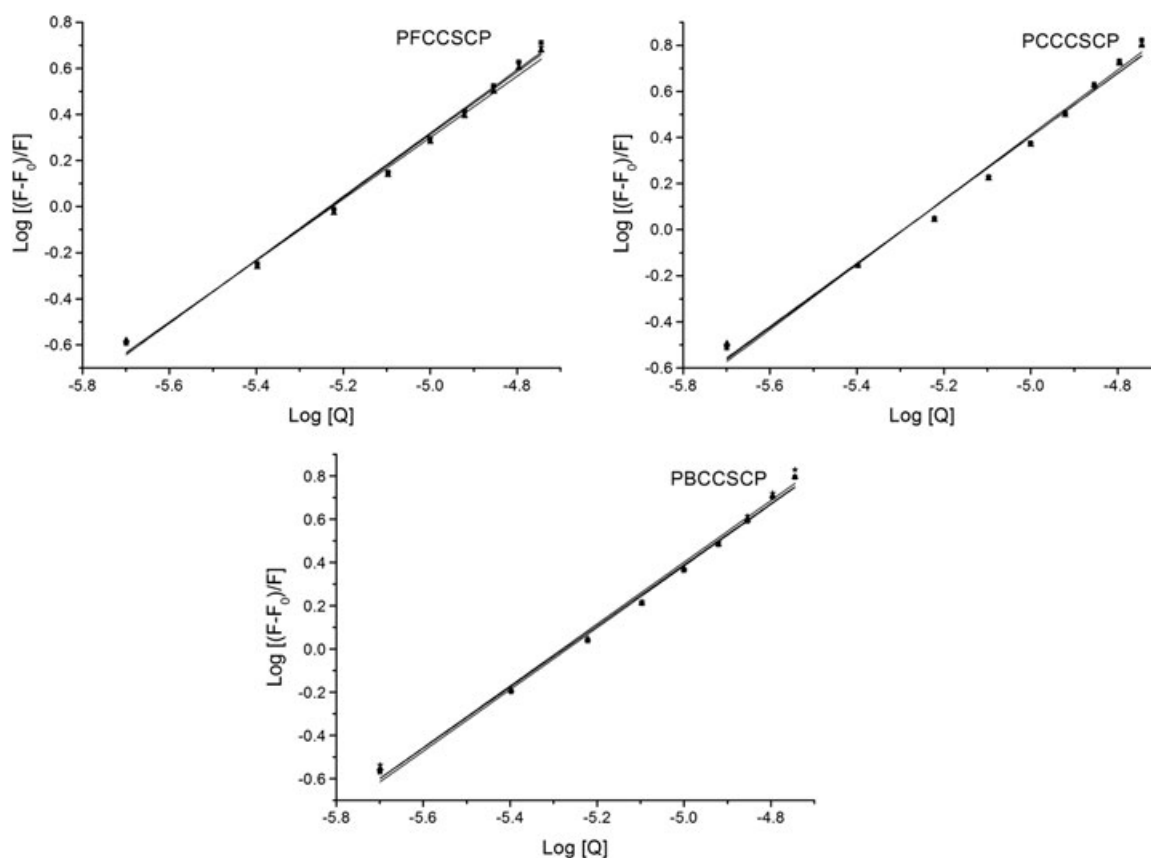


Figure 4. Plots of $\lg [(F_0 - F)/F]$ versus $\log [Q]$ at different temperatures

Table 4. Binding constants and number of binding sites of CCSCPs to BSA

		BSA-PFCCSCP	BSA-PCCCSCP	BSA-PBCCSCP
T = 298 K	Log (K_A)	7.19(20)	7.44(26)	7.52(19)
	$K_A \times 10^7$ (M^{-1})	1.54	2.76	3.33
	n	1.37(4)	1.41(5)	1.43(4)
	R	0.9973	0.9956	0.9975
T = 303 K	Log (K_A)	7.13(19)	7.31(23)	7.55(25)
	$K_A \times 10^7$ (M^{-1})	1.35	2.04	3.54
	n	1.36(4)	1.38(5)	1.43(5)
	R	0.9974	0.9963	0.9958
T = 308 K	Log (K_A)	6.97(20)	7.27(27)	7.47(20)
	$K_A \times 10^7$ (M^{-1})	0.94	1.86	2.93
	n	1.33(4)	1.37(5)	1.42(4)
	R	0.9969	0.9950	0.9974

Table 5. Thermodynamic parameters of BSA-CCSCP

System	ΔG ($kJ \cdot mol^{-1}$)			ΔH ($kJ \cdot mol^{-1}$)	ΔS ($J \cdot mol^{-1} \cdot K$)
	T = 298 K	T = 303 K	T = 308 K		
BSA-PFCCSCP	-41.01	-41.37	-41.11	-37.89	10.82
BSA-PCCCSCP	-42.45	-42.40	-42.86	-30.30	40.50
BSA-PBCCSCP	-42.92	-43.79	-44.03	-9.60	112.16

which temperature or for different CCSCPs were around -42 $kJ \cdot mol^{-1}$, which revealed that the binding process was spontaneous. Although all CCSCPs had negative ΔH and positive ΔS , the

contributions of ΔH and ΔS to ΔG values differed for the three CCSCPs. From PFCCSCP to PBCCSCP, the contributions of ΔS increased greatly followed by the steep dipping of ΔH° in the

values of their ΔG . This phenomenon indicated that the interaction forces in BSA–PFCCSCP and BSA–PCCSCCP systems were van der Waals interactions and hydrogen bonds. When 4'-substituent in CCSCP structure was changed to bromine, the ionic interaction and proton transfer could control the overall energetics (15).

Energy transfer between BSA and CCSCP

Resonance energy transfer (RET) is another important process occurring in the excited state. This process occurs when the emission spectrum of the donor overlaps with the absorption spectrum of the acceptor. Unlike other fluorescence phenomena, RET does not depend on interactions of the fluorophore with other molecules in the surrounding solvent shell. According to Förster theory (5,16), non-radioactive energy transfer is effective over much longer distances and the intervening solvent or macromolecule have few effects on the efficiency of energy transfer, which depends primarily on the donor-to-acceptor (D–A) distance. The extent of energy transfer is determined by the distance between the donor and acceptor and the extent of spectral overlap. The efficiency of energy transfer (E) was related to the D–A distance and it could be calculated using equation (6):

$$E = 1 - \frac{F}{F_0} = \frac{R_0^6}{R_0^6 + r^6} \quad (6)$$

where R_0 is the Förster distance when the efficiency of resonance energy transfer is 50% and r is the D–A distance. The value of R_0 can be calculated using equation (7):

$$R_0^6 = 8.79 \times 10^{-25} \kappa^2 \Phi N^4 J \quad (7)$$

where κ^2 is spatial orientation factor of the dipole, N is the refractive index of the medium in the wavelength range where the spectral overlap is significant, Φ is the fluorescence quantum yield of the donor in the absence of acceptor, and J is the overlap integral of the fluorescence emission spectrum of the donor and the absorption spectrum of the acceptor as in equation (8):

$$J = \frac{\sum F(\lambda)\varepsilon(\lambda)\lambda^4 \Delta\lambda}{\sum F(\lambda)\Delta\lambda} \quad (8)$$

where $F(\lambda)$ is the fluorescence intensity of the fluorescence donor at wavelength λ and $\varepsilon(\lambda)$ is the molar absorbance of the acceptor at wavelength λ . The overlap of the fluorescence emission spectra of BSA and the absorption spectra of CCSCPs at 298 K are shown in Figure 5.

Under the above experimental conditions, $\kappa^2 = 2/3$, N was the average value of water and organic solute (1.366) and $\Phi = 0.118$ (10,16). According to equations (6–8), the values of the parameters are listed in Table 6. The binding distances of three CCSCPs were less than 8 nm and $0.5R_0 < r < 1.5R_0$, which indicated that the energy transfer from BSA to CCSCPs occurred with high probability (9,16). Furthermore, three CCSCPs had a similar ability to bind with BSA because of nearly same binding distances.

Table 6. Distance parameters between BSA and CCSCPs

System	J ($\text{cm}^3 \cdot \text{M}^{-1}$)	E	R_0 (nm)	r (nm)
BSA–PFCCSCP	1.51×10^{-14}	0.66	2.59	2.31
BSA–PCCSCSCP	1.70×10^{-14}	0.70	2.64	2.29
BSA–PBCCSCP	1.75×10^{-14}	0.70	2.65	2.31

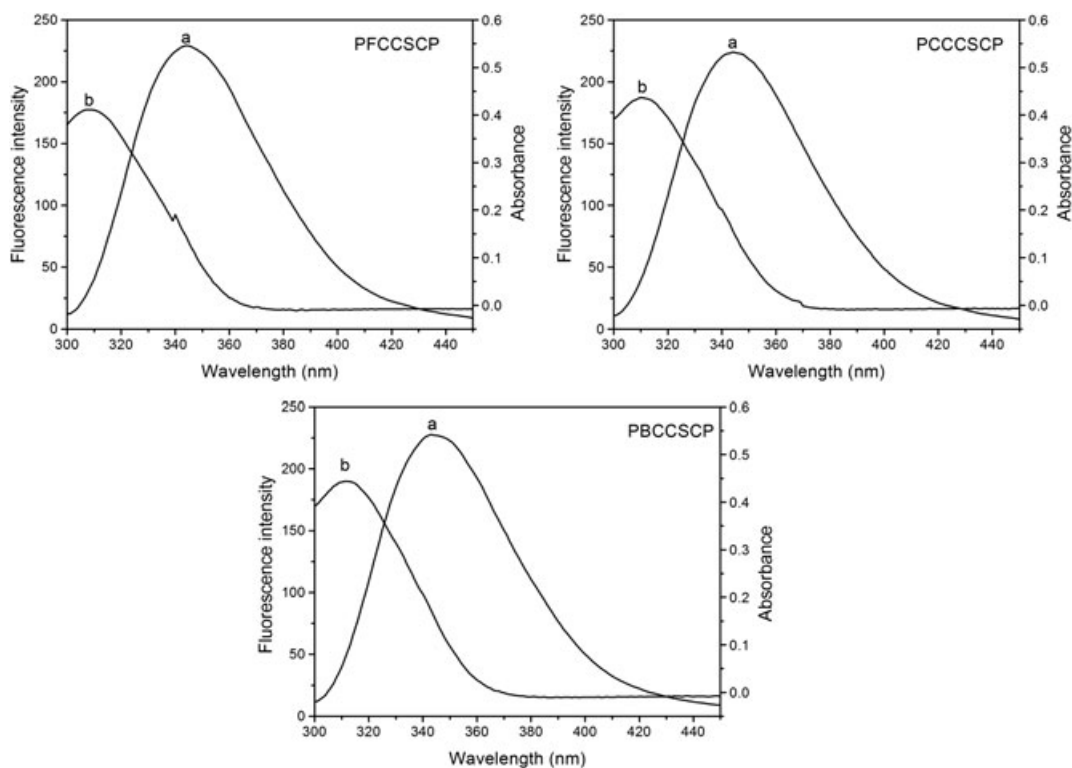


Figure 5. Overlap of fluorescence emission spectrum of BSA (a) and absorption spectrum of CCSCPs (b). $c(\text{BSA}) = c(\text{CCSCP}) = 1.00 \times 10^{-5}$ M; $T = 298$ K

Conformation change

Since synchronous fluorescence can give narrow and simple spectra, it was used to provide information about the molecular environment in the vicinity of the molecules and evaluate the conformational changes of BSA. By measuring the shift of emission maximum, the environment of amino acid residues in BSA could be studied and the shifts corresponded to the changes of the polarity around the molecule (9). The characteristic information for tyrosine or tryptophan residues was given by the synchronous fluorescence, when the difference between excitation wavelength and emission wavelength were stabilized at 15 or 60 nm (17). The effects of CCSCPs on the synchronous fluorescence spectra of BSA are shown in Figure 6. It is apparent from Figure 6 that the maximum emission wavelengths of tyrosine residues slightly shifted towards shorter wavelengths (left column, Figure 6) and the maximum emission wavelengths

of tryptophan residues stabled at 350 nm. These results indicate that CCSCPs did not affect the microenvironment of tryptophan residues during the binding process and the polarity around the tyrosine residues decreased and hydrophobicity around tyrosine residues increased (4,9).

Conclusions

In this paper, the interactions of CCSCPs and BSA were investigated by fluorescence and ultraviolet spectroscopy. The experimental results indicate that the three CCSCPs formed complexes with BSA at low concentrations at three temperatures. A combined quenching (static and dynamic) process occurred at higher concentrations of CCSCPs. Based on thermodynamic parameters, hydrophobic and electrostatic interactions were the main binding forces in the BSA–PFCCSCP and BSA–PCCCS

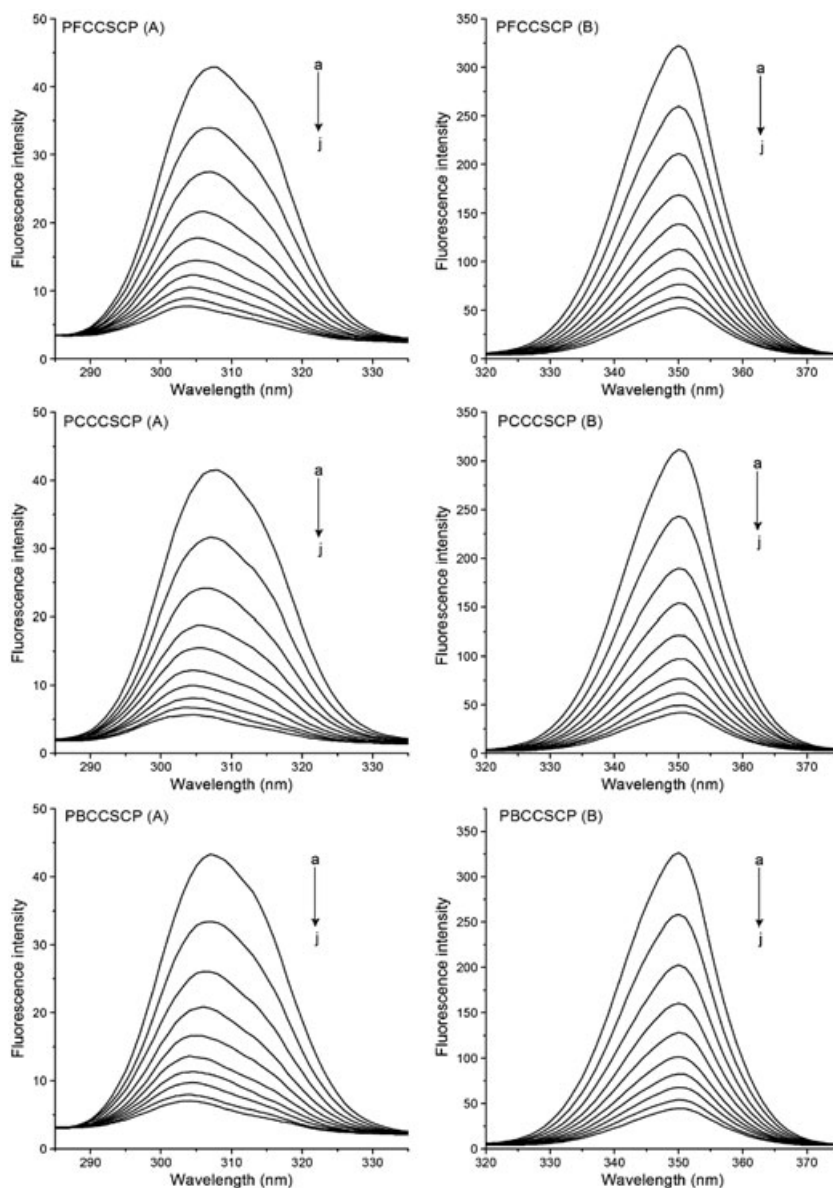


Figure 6. Synchronous fluorescence spectra of BSA in the present CCSCPs. (A) $\Delta\lambda = 15$ nm, (B) $\Delta\lambda = 60$ nm; $T = 298$ K; $c(\text{BSA}) = 1.00 \times 10^{-5}$ M; $c(\text{CCSCP}) / (\times 10^{-5} \text{ M})$, (a–j) 0.00, 0.20, 0.40, 0.60, 0.80, 1.00, 1.20, 1.40, 1.60 and 1.80, respectively

systems, but the ionic interactions and proton transfer played major roles in the binding process of the BSA-PBCCSCP system. The average binding distances of CCSCPs were around 2.3 nm, indicating that the energy transfer from BSA to CCSCPs occurred with high possibility. Moreover, the measured synchronous fluorescence spectroscopy indicated that the conformation of BSA was changed in the presence of CCSCPs and that binding occurred at tyrosine residues of BSA. The knowledge obtained in this study can provide information to understand the mode of action between CCSCPs and BSA and could be beneficial to drug design and pharmaceutical research.

Acknowledgements

This work was supported by a grant from the National Natural Science Foundation of China (20962002, 20662001).

References

1. Huang K, Ding Z, Zhao S, Yan Y. *Compendium of Modern Materia Medica*, Beijing, China: Medical Science Press, 2001.
2. Huang L, Lin C, Li A, Wei B, Teng J, Li L. Pro-coagulant activity of phenolic acids isolated from *Blumea riparia*. *Nat Prod Commun* 2010;5:1263–66.
3. Yu M, Ding Z, Jiang F, Ding X, Sun J, Chen S, et al. Analysis of binding interaction between pegylated puerarin and bovine serum albumin by spectroscopic methods and dynamic light scattering. *Spectrochim Acta, Part A* 2011;83:453–60.
4. Yu X, Liu R, Yi R, Yang F, Huang H, Chen J, et al. Study of the interaction between N-confused porphyrin and bovine serum albumin by fluorescence spectroscopy. *Spectrochim Acta, Part A* 2011;78:1329–35.
5. Naik PN, Chimatadar SA, Nandibewoor ST. Study on the interaction between antibacterial drug and bovine serum albumin: A spectroscopic approach. *Spectrochim Acta, Part A* 2009;64:841–5.
6. Carter DC, Ho JX. Structure of serum albumin. *Adv Protein Chem* 1994;45:153–203.
7. Tian J, Liu J, Zhang J, Hu Z, Chen X. Fluorescence studies on the interactions of barbaloin with bovine serum albumin. *Chem Pharm Bull* 2003;51:579–82.
8. He XM, Carter DC. Atomic structure and chemistry of human serum albumin. *Nature* (London, U K) 1992;358:209–15.
9. Guo X-J, Sun X-D, Xu S-K. Spectroscopic investigation of the interaction between riboflavin and bovine serum albumin. *J Mol Struct* 2009;931:55–9.
10. Lakowicz JR. *Principles of Fluorescence Spectroscopy*. three ed. New York Springer, 2010.
11. Zhao G-J, Han K-L. Hydrogen bonding in the electronic excited state. *Acc Chem Res* 2012;45:404–13.
12. Yuan T, Weljie AM, Vogel HJ. Tryptophan fluorescence quenching by methionine and selenomethionine residues of calmodulin: orientation of peptide and protein binding. *Biochemistry* 1998;37:3187–95.
13. Bi S, Sun Y, Qiao C, Zhang H, Liu C. Binding of several anti-tumor drugs to bovine serum albumin: Fluorescence study. *J Lumin* 2009;129:541–7.
14. Jiang M, Xie MX, Zheng D, Liu Y, Li XY, Chen X. Spectroscopic studies on the interaction of cinnamic acid and its hydroxyl derivatives with human serum albumin. *J Mol Struct* 2004;692:71–80.
15. Ross PD, Subramanian S. Thermodynamics of protein association reactions: forces contributing to stability. *Biochemistry* 1981;20:3096–102.
16. Kang J, Liu Y, Xie MX, Li S, Jiang M, Wang YD. Interactions of human serum albumin with chlorogenic acid and ferulic acid. *Biochim Biophys Acta, Gen Subj* 2004;1674:205–14.
17. Burstein EA, Vedenkina NS, Ivkova MN. Fluorescence and the location of tryptophan residues in protein molecules. *Photochem Photobiol* 1973;18:263–79.